Prediction of Iron K-Edge Absorption Spectra Using Time-Dependent Density Functional Theory[†]

Serena DeBeer George,*,‡ Taras Petrenko,§ and Frank Neese*,§

Stanford Synchrotron Radiation Laboratory, SLAC, Stanford University, Stanford, California 94309, and Institut für Physikalische und Theoretische Chemie, Universität Bonn, Wegelerstrasse 12, D-53115 Bonn, Germany

Received: April 12, 2008; Revised Manuscript Received: June 7, 2008

Iron K-edge X-ray absorption pre-edge features have been calculated using a time-dependent density functional approach. The influence of functional, solvation, and relativistic effects on the calculated energies and intensities has been examined by correlation of the calculated parameters to experimental data on a series of 10 iron model complexes, which span a range of high-spin and low-spin ferrous and ferric complexes in O_h to T_d geometries. Both quadrupole and dipole contributions to the spectra have been calculated. We find that good agreement between theory and experiment is obtained by using the BP86 functional with the CP(PPP) basis set on the Fe and TZVP one of the remaining atoms. Inclusion of solvation yields a small improvement in the calculated energies. However, the inclusion of scalar relativistic effects did not yield any improved correlation with experiment. The use of these methods to uniquely assign individual spectral transitions and to examine experimental contributions to backbonding is discussed.

Introduction

Metal K-edge X-ray absorption spectroscopy (XAS) is a powerful probe of the electronic and geometric structure of iron sites in inorganic and biological systems.[1,2] In particular, the Fe K-pre-edge region of the XAS spectrum provides information on the oxidation state, geometry, and, in some cases, spin state of the iron atom. An XAS edge results when a core electron absorbs an energy equal to or greater than its binding energy. In the case of an Fe K-edge, this corresponds to ~7.1 keV, the binding energy of an Fe 1s electron. The pre-edge feature of an XAS spectrum is formally a 1s to 3d quadrupole allowed transition, which as such is much weaker than the dipole-allowed 1s to 4p "main" edge transition. However, distortions from centrosymmetry allow for 4p character to mix into the metal 3d orbitals giving this transition electric dipole-allowed character and thus increasing the pre-edge intensity.[3−5] Hence, in a six-coordinate octahedral limit, where metal 3d and 4p orbitals cannot mix due to symmetry constraints, a very weak pre-edge feature is observed. Whereas in a five-coordinate C_{4v} structure, where $4p_{x,y,z}$ orbitals can mix with the metal $3d_{xz}$,d_{yz}, and d_{z^2} orbitals, a mechanism for significantly increased pre-edge intensity is provided.[2] This allows for the use of pre-edge intensities as a way to experimentally determine coordination numbers. As errors in the coordination numbers determined by extended X-ray absorption fine structure (EXAFS) are known to be large (on the order of 20−25%),[6] the ability to limit the solution space and obtain further insight into the local geometry of the iron site is greatly enhanced by understanding the pre-edge. It also provides experimental insight into the local geometric structure in cases where EXAFS may not be obtainable.

The inverse relationship between pre-edge intensity and coordination number was first noted by Roe et al., based on a systematic study of 28 synthetic iron compounds.[1] The experimental data were correlated to extended Hückel calculations, and it was demonstrated that the pre-edge intensity showed a near linear relationship with the total 4p character mixed into the 3d orbitals. Later, Westre et al. examined Fe K-pre-edge features in greater detail, developing a methodology to understand the energy splittings and intensity distributions based on ligand field theory.[2] Using the pre-edge intensity of octahedral complexes as an experimental limit of a quadrupole-only transition, the quadrupole intensity was experimentally estimated and the remaining intensity was assigned to metal 4p character. More recently, Arrio and co-workers have calculated quadrupole transition intensities in iron minerals using a ligand field multiplet approach.[7] These studies have served as benchmarks for our understanding of Fe K-edge spectra and have provided important references for the understanding of numerous non-heme iron enzymes[8−10] and related model complexes.[11−16]

Fe K-edge XAS has also had an important impact on our understanding of high-valent iron intermediates. Studies by Que and co-workers have clearly shown that Fe(IV)-oxo and nitrido model complexes are characterized by pre-edge features that are to higher energy and have greater intensity than known ferrous or ferric complexes.[13,14,16] The increased intensity may be attributed to the very short Fe-oxo/nitrido bonds in these complexes, which provide a mechanism metal $4p_z$-d_{z^2} mixing via overlap with the oxygen or nitrogen 2p orbitals.[17] The increased energy may be attributed to increased ligand field. Recent work by Wieghardt and co-workers on Fe(V) and Fe(VI) nitrido complexes shows a similar trend, with the pre-edge intensity increasing as the Fe-nitrido bond becomes shorter and the transition energy increasing by ~1 eV per unit of oxidation state.[11,12] Parallel observations have been made for the XAS data of a recently reported Fe(V)-oxo complex.[15]

Although it is clear that our understanding of Fe K-pre-edge features has greatly matured, the interpretation of these features

---

[†] Part of the "Sason S. Shaik Festschrift".

* To whom correspondence should be addressed. E-mail: (S.D.G.) debeer@stanford.edu and (F.N.) neese@thch.uni-bonn.de.

[‡] Stanford University.

[§] Universität Bonn.

10.1021/jp803174m CCC: $40.75

is often still based on a combination of theoretical and empirical trends. Although clear correlations of the experimental data to calculated 3d-4p mixing have been made,[1,2] there are relatively few studies on the calculation of quadrupole transition intensities,[7] and to our knowledge, a systematic study of iron K-pre-edge features using a time-dependent density functional theory (TD-DFT) has not been made. In addition, previous studies have not included the calculation of pre-edge energies.

As an understanding of the pre-edge energies and intensities is essential to fully understanding the electronic structure, we therefore feel that it is of general utility to calculate these parameters directly using a TD-DFT approach. In a previous paper, we have outlined a simple, efficient, and yet successful TD-DFT approach and have successfully applied it to the prediction of Cl[18] and S[19] and K-edge spectra. In ref 18, we have also discussed the important subject of quadrupole contributions to the XAS oscillator strength in some detail including the issue of gauge noninvariance. In this paper, we present a similar calibration for the calculation of Fe K-pre-edge features, including dipole and quadrupole transition intensities and energies. We have systematically examined the influence of functional, solvation, and relativistic effects on the calculated parameters. We have chosen a set of test complexes based on data previously published by Westre et al.,[2] which spans a range of high-spin and low-spin ferrous and ferric complexes in varying geometries.

Theory

In DFT linear response theory, the transition frequencies ω are calculated from the nonstandard eigenvalue type equation:[20,21]

$$\begin{pmatrix} \mathbf{A} & \mathbf{B} \\ \mathbf{B} & \mathbf{A} \end{pmatrix}\begin{pmatrix} \mathbf{X} \\ \mathbf{Y} \end{pmatrix} = \omega \begin{pmatrix} \mathbf{1} & \mathbf{0} \\ \mathbf{0} & \mathbf{-1} \end{pmatrix}\begin{pmatrix} \mathbf{X} \\ \mathbf{Y} \end{pmatrix} \tag{1}$$

With the supermatrices

$$A_{ia,jb} = (\varepsilon_a - \varepsilon_i)\delta_{ai,jb} + \left(ia|\tilde{f}_{\mathrm{XC}}|jb\right) - c_{\mathrm{HF}}\left(ij|r_{12}^{-1}|ab\right) \tag{2}$$

$$B_{ia,jb} = \left(ia|\tilde{f}_{\mathrm{XC}}|jb\right) - c_{\mathrm{HF}}\left(jc|r_{12}^{-1}|kb\right) \tag{3}$$

And the effective two-electron exchange-correlation operator:

$$\tilde{f}_{\mathrm{XC}}(\mathbf{r}_1, \mathbf{r}_2) = r_{12}^{-1} + \frac{\delta^2 E_{\mathrm{XC}}}{\delta\rho(\mathbf{r}_1)\delta\rho(\mathbf{r}_2)} \tag{4}$$

For some two-electron operator $g(\mathbf{r}_1,\mathbf{r}_2)$, the integrals are defined as:

$$(pq|g|rs) = \int\int \psi_p(\mathbf{r}_1)\psi_q(\mathbf{r}_1)g(\mathbf{r}_1, \mathbf{r}_2)\psi_r(\mathbf{r}_2)\psi_s(\mathbf{r}_2)\,\mathrm{d}\mathbf{r}_1\,\mathrm{d}\mathbf{r}_2 \tag{5}$$

Labels i and j refer to occupied spin orbitals of the Kohn−Sham solution, a and b refer to unoccupied orbitals (p, q, r, and s to general spin orbitals), ε_p is the orbital energy, and c_{HF} is the fraction of Hartree−Fock exchange in the density functional. E_{XC} is the exchange correlation functional, $\rho(\mathbf{r}_1)$ is the ground-state electron density at position $\mathbf{r}_1$, and r_{12} is the interelectronic distance.

The solution of eq 1 yields the transition frequencies ω transition amplitudes X_{ai},Y_{ai} from which one can calculate dipole and quadrupole transition moments as:

$$\mathbf{D} = \sum_{ia} (X_{ia} + Y_{ia})(i|\hat{\mathbf{D}}|a) \tag{6}$$

$$\mathbf{Q} = \sum_{ia} (X_{ia} + Y_{ia})(i|\hat{\mathbf{Q}}|a) \tag{7}$$

$$\hat{D}_k = -r_k \tag{8}$$

$$\hat{Q}_{kl} = \left(r_k r_l - \frac{1}{3} r^2 \delta_{kl}\right) \tag{9}$$

where the sum $\mathbf{r}$ is the position operator of the electron with components r_k [$k = x,y,z$ and $r = (r_x^2 + r_y^2 + r_z^2)^{1/2}$]. The calculation of transition dipole moments is straightforward, but the calculation of quadrupole transition moments presents some difficulty, since the results depend on the choice of origin. In ref 18, we have examined this problem in more detail. Because the quadrupole transition moment mechanism arises from a series expansion, it seems natural to choose the origin such that the expansion yields optimum convergence. As discussed in detail in ref 18, it is possible to readjust the origin, $\mathbf{R}$, for each transition (I) from the solution of a simple linear equation system as:

$$\mathbf{A}^{(I)}\mathbf{R} = \mathbf{C}^{(I)} \tag{10}$$

With

$$A_{kl}^{(I)} = \frac{8}{15}\omega_I|\mathbf{D}^{(I)}|^2\delta_{kl} - \frac{4}{15}\omega_I D_k^{(I)} D_l^{(I)} \tag{11}$$

$$C_k = \frac{1}{5}\omega_I \sum_l Q_{kl}^{(I)} D_l^{(I)} - \frac{2}{3}\sum_{lm} \varepsilon_{klm} M_l^{(I)} D_m^{(I)} \tag{12}$$

Here, ε_{klm} is the Levi−Civitta tensor and M_l is the magnetic transition dipole moment. This procedure was followed throughout the present work.

It is possible to simplify eq 1 by neglecting the **B**-matrix (or alternatively constraining **Y** to be zero). This was first discussed by Head-Gordon and co-workers[22] and amounts to the Tamm−Dancoff approximation (TDA). One then simply solves:

$$\mathbf{AX} = \omega\mathbf{X} \tag{13}$$

which resembles the configuration interaction with a single excitation approach. Our implementation of these equations has been discussed in detail in refs 23 and 24. The TDA was applied throughout the present work. (Results obtained with the full TD-DFT response equations are almost indistinguishable from the TD-DFT/TDA results with respect to transition energies as well as oscillator strengths.) In solving eq 13, we have projected the solution onto the manifold of core-excited single excitations. This obviously neglects the coupling of the core-excited K-edge states to L- and M-edges, as well as valence excited states. This appears to be a plausible approximation due to the large energy difference between the zeroth order states and the small coupling matrix elements. From perturbation theory, the coupling between a core-level excited state 1s→a and a valence excitation j_v→b is on the order of

$$X_{1s-a,j_v-b} \approx -[(1s, a|\tilde{f}_{\mathrm{XC}}|jb) - c_{\mathrm{HF}}(1s, j|r_{12}^{-1}|ab)]\Delta_{1s-a,j-b}^{-1} \tag{14}$$

which involves the interaction of a very small transition density $\rho_{1s,a}(\mathbf{r}) = \psi_{is}(\mathbf{r})\psi_a(\mathbf{r})$ (concentrated in the core region) with a possibly larger transition density $\rho_{j_v},a(\mathbf{r}) = \psi_{j_v}(\mathbf{r})\psi_b(\mathbf{r})$ (concentrated in the valence region). Even for the presumably largest case $a = b$, the differential overlap between a core 1s and a valence j_v function is expected to be small, such that the numerator is expected to be small, and the admixture of the valence excited excitation into the final core-level excited state is further damped by the large energy denominator $\Delta_{1s-a,j-b}^{-1}$ that measures the zeroth-order energy difference between the two single excitations 1s→a and j_v→b. In particular, the effect on the transition intensity should be very small since it is at

TABLE 1: Oxidation States, Spin States, and Geometries of Investigated Model Complexes

complex	Fe oxidation state	spin state	geometry
$[FeCl_4]^{1-}$	III	5/2	T_d
$[FeCl_4]^{2-}$	II	2	T_d
$[FeCl_6]^{3-}$	III	5/2	O_h
$[FeCl_6]^{4-}$	II	2	O_h
$[Fe(acac)_3]^0$	III	5/2	O_h
$[Fe(salen)Cl]^0$	III	5/2	C_{4v}
$[Fe(CN)_6]^{3-}$	III	1/2	O_h
$[Fe(CN)_6]^{4-}$	II	0	O_h
$[Fe(prpep)_2]+$	III	1/2	O_h
$[Fe(prpep)_2]^0$	II	0	O_h

TABLE 2: Combination of Technical Parameters Tested in the Present Work

method	functional	structure	relativistics	solvation
1	BP86	X-ray	none	COSMO
2	B3LYP	X-ray	none	COSMO
3	BP86	X-ray	none	none
4	BP86	X-ray	ZORA	COSMO
5	BP86	X-ray	DKH2	COSMO
6	BP86	Opt	none	COSMO

best quadratic in the (small) mixing coefficient, and the dominant correction is proportional to its fourth power. Thus, what remains is the very limited shift of the transition energy of the core-level excited state due to the interaction with the valence excitation. The shift of the transition energy is likely to be negligible as compared to the inherent errors of the methodology, in particular in the description of the bonding region.

Computational Details

A series of Fe complexes for which Fe K-edge data are available in the literature were systematically investigated using a TD-DFT approach as implemented in the ORCA package.[25] These include $[FeCl_4]^{1-/2-}$,[26,27] $[FeCl_6]^{3-/4-}$,[28] $[Fe(acac)_3]^0$ (where acac = acetylacetonate),[29] $[Fe(salen)Cl]^0$ [where H_2salen = *N*,*N*′-bis(salicylidene)ethylendiamine],[30] $[Fe(CN)_6]^{3-/4-}$,[31,32] $[Fe(prpep)_2]^{+/0}$ {where Hprpep = N[−2-(4-imidazolyl)ethyl]pyrimidine-4-carboxyamide}.[33] The oxidation state, spin state, and local geometry of the model complexes are given in Table 1.

The Fe K-edge pre-edge spectra of all complexes were calculated by first carrying out spin unrestricted ground-state calculations at the experimental X-ray structures. For these calculations, the BP86 functional[34,35] was used in combination with the CP(PPP) basis set[36] for the metal and the TZVP basis set[37] for all other atoms. Following the ground-state DFT, TD-DFT calculations were performed, allowing only for excitations from the Fe-1s orbitals. Calculations were carried out in a dielectric continuum using the conductor like screening model (COSMO)[38] in an infinite dielectric.

To systematically test the effect of the functional, solvation, and relativistics, the above calculations (referred to as method 1) were repeated with the modifications described below. As previous work on chlorine[18] and sulfur[19] has established the use of the CP(PPP) basis set for the metal and the TZVP basis set for the remaining atoms to be most successful, the effect of basis set was not further explored in the present study. We have defined six methods that we have applied to all complexes in this series and that are described in Table 2.

The ZORA calculations were performed according to van Wüllen's model potential method[39] as implemented in ORCA, while in the DKH2 calculations,[40,41] we followed the accepted practice to only transform the one-electron part of the Hamiltonian. In method 6, the geometries were optimized at the BP86/TZVP level.

Results and Analysis

XAS Pre-Edge Energies and Intensities (Method 1). The previously reported experimental Fe K-pre-edge intensities and energies of the 10 model complexes[2] and the corresponding calculated parameters (using method 1) are summarized in Table 3. Figure 1 shows the relationship between the calculated total oscillator strength (dipole + quadrupole contribution) and the experimental intensities.[42] The linear relationship has been used to scale the calculated areas for better comparison with the experimental data. A linear correlation coefficient of 0.98 is obtained for the experimental areas relative to the calculated intensities showing excellent agreement at this level of theory. Naturally, the largest deviations from experiment occur for the complexes that have very low pre-edge intensities. Here, many subtle effects like vibronic effects, spin−orbit coupling, or low-symmetry distortions induced by the environment may influence the experimental intensities but are not included in the theoretical model. The scaled values are listed as "predicted areas" in Table 3.

TABLE 3: Comparison of Experimental Energies and Intensities to Calculated Values

	experimental[a]			calculated[c]					
compound	*E*, p1[b]	*E*, p2	area	*E*, p1	*E*, p2	dipole	quadrupole	total	predicted area[d]
$[Fe(III)Cl_4]^{1-}$	7113.2		20.7	7113.2		0.1439	0.0207	0.1646	20.5
$[Fe(II)Cl_4]^{2-}$	7111.6	7113.1	12.9	7111.8	7112.5	0.0869	0.0116	0.0985	13.4
$[Fe(III)Cl_6]^{3-}$	7112.8	7114	4	7113.1	7113.9	0.0000	0.0234	0.0234	5.2
$[Fe(II)Cl_6]^{4-}$	7111.8	7113.4	3.6	7112	7113	0.0000	0.0193	0.0193	4.8
$[Fe(III)(acac)_3]^0$	7112.8	7114.3	4.6	7112.5	7114.3	0.0178	0.0143	0.0321	6.2
$[Fe(salen)Cl]^0$	7112.9		14.4	7112.9		0.0951	0.0069	0.1020	13.7
$[Fe(CN)_6]^{3-}$	7110.1	7113.3	5.2	7110.7	7114.2	0.0005	0.0123	0.0128	4.1
$[Fe(CN)_6]^{4-}$	7112.9		4.2	7114		0.0000	0.0177	0.0177	4.6
$[Fe(prpep)_2]^+$	7111	7112.7	6.4	7111.4	7112.7	0.0080	0.0086	0.0165	4.5
$[Fe(prpep)_2]^0$	7112.1		5.3	7112.1[e]		0.0049	0.0098	0.0147	4.3

[a] Experimental energies and areas as reported in ref 2. [b] All energies are reported in eV. *E*, p1 = energy of the first peak, and *E*, p2 = energy of the second peak. [c] Calculated dipole and quadrupole contributions are reported. [d] Predicted areas are based on establishing a linear relationship between the total calculated (dipole plus quadrupole) contributions and the experimental areas. For method 1, used was the following relation: predicted area = 2.7304 + (108.77 × (calculated dipole + quadrupole contributions)). [e] Two peaks are calculated for $[Fe(II)(prpep)_2]^0$, one at 7111.4 and one at 7112.7. Applying a broadening of 2 eV to the calculated spectra results in a single peak at 7112.1 eV.

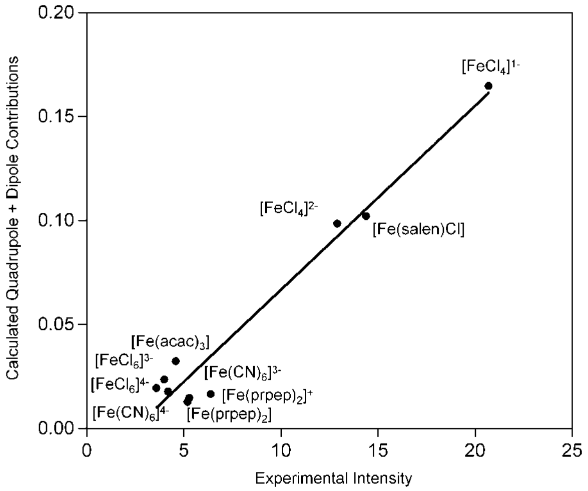

Figure 1. Relationship of the calculated dipole and quadrupole intensities (using method 1) to the experimental pre-edge intensities.

It is expected the calculated energies are underestimated due to limitations of DFT in modeling the potentials near the nucleus, which results in an Fe 1s orbital that is too high in energy relative to the valence orbitals.[43] The opposite bias is induced by the neglect of scalar relativistic effects. These effects are known to stabilize s- (and p-) orbitals and destabilize d-orbitals.[44] Thus, they will serve to increase the transition energies as compared to the nonrelativistic limit. In our opinion, the only chemically relevant quantities are *relative* transition energies, for example, the shifts in the transition energies from one complex to another as well as the splittings between several resolved (or unresolved) pre-edge peaks. Thus, once a basis set and functional are chosen, one can determine once and for all a constant energy shift that can be applied to all calculated transition energies to ease the comparison with experiment. For method 1, all calculated energies in Table 3 have been shifted by a constant value of 171.3 eV. The average energy shifts required to align the calculated pre-edge spectra with the experimental data (for both peak 1 and peak 2 of the pre-edge region) for all tested methods are presented in Table 4. In addition, Table 4 shows the linear correlation coefficient for the calculated vs the experimental areas for each method. For method 1, the average absolute deviation in calculated energies is 0.4 eV over the series of 10 complexes. This value decreases to 0.3 eV if only the cationic, neutral, monoanionic, and dianionic complexes are included in the correlation. Highly anionic molecules are difficult to treat accurately by quantum chemical methods since they are not stable under gas phase conditions, which means that the highest occupied orbitals have positive energies (hence they are unbound); thus, the calculations become very basis set-dependent. Hence, one should generally view the results of such calculations with caution. Detailed treatments of the Madelung field at the site of the complex with in the crystal environment would likely provide more accurate results for such highly charged complexes. However, this would require dedicated solid state techniques that are presently not available to us.[45]

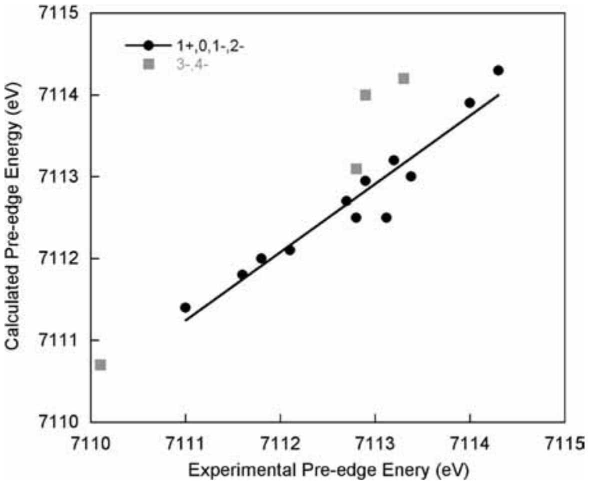

Figure 2. TD-DFT calculated vs experimental energies, using method 1. Calculated values have been shifted by a constant value of 171.3 eV. Black dots correspond to dianionic complexes, Gray squares correspond to trianionic and tetraanionic complexes.

Nevertheless, Figure 2 establishes a linear relation between experimental and calculated energies, with a linear correlation coefficient of 0.95 if the highly negatively charged (tri- and tetra-anionic) complexes (shown as gray squares, Figure 3) are excluded from the series.

Having established a linear correlation between experimental intensities and energies, it is instructive to examine the experimental data relative to the calculated spectra. Figure 3 shows the experimental data for the high-spin (top, left) and low-spin (top, right) complexes as compared to the corresponding calculated spectra (bottom). These plots illustrate that not only are the experimental intensities and energies well-reproduced, but importantly, the relative energy splitting and intensity distribution are also well-predicted.

Effect of the Functional (Method 2). The impact of the functional used in the calculations on both the calculated energies and the intensities was tested by using the B3LYP instead of BP86 (method 2). Table summarizes these results. The relationship between calculated and experimental intensity remains linear, with the linear correlation coefficient decreasing slightly to 0.96. The average shift required to align the calculated spectra to the experimental data decreases to 143.3 eV. This may be expected on the basis that the admixture of Hartree—

TABLE 4: Calculated Energies and Intensities Relative to Experimental Values

	for all complexes		for complexes with 1+, 0, 1, 1−, and 2− total charge	
method	avg energy shift[a]	*R* value for intensity[b]	avg energy shift[a]	*R* value for intensity[b]
1	171.1 (0.4)	0.98	171.3 (0.3)	0.98
2	143.3 (1.1)	0.96	143.3 (0.4)	0.97
3	171.0 (0.5)	0.98	171.2 (0.3)	0.98
4	2.3 (2.2)	0.95	2.2 (1.5)	0.98
5	105.6 (0.5)	0.98	105.6 (0.5)	0.97
6	170.9 (0.3)	0.99	170.9 (0.3)	0.99

[a] The energy reported is the shift required to match the calculated transition to experiment. Values are reported for both p1 and p2, as given in Table 2. In all cases, the calculation underestimates the transition energy. The number in parentheses is the standard deviation. [b] The *R* value is the linear correlation coefficient for the calculated vs experimental intensities.

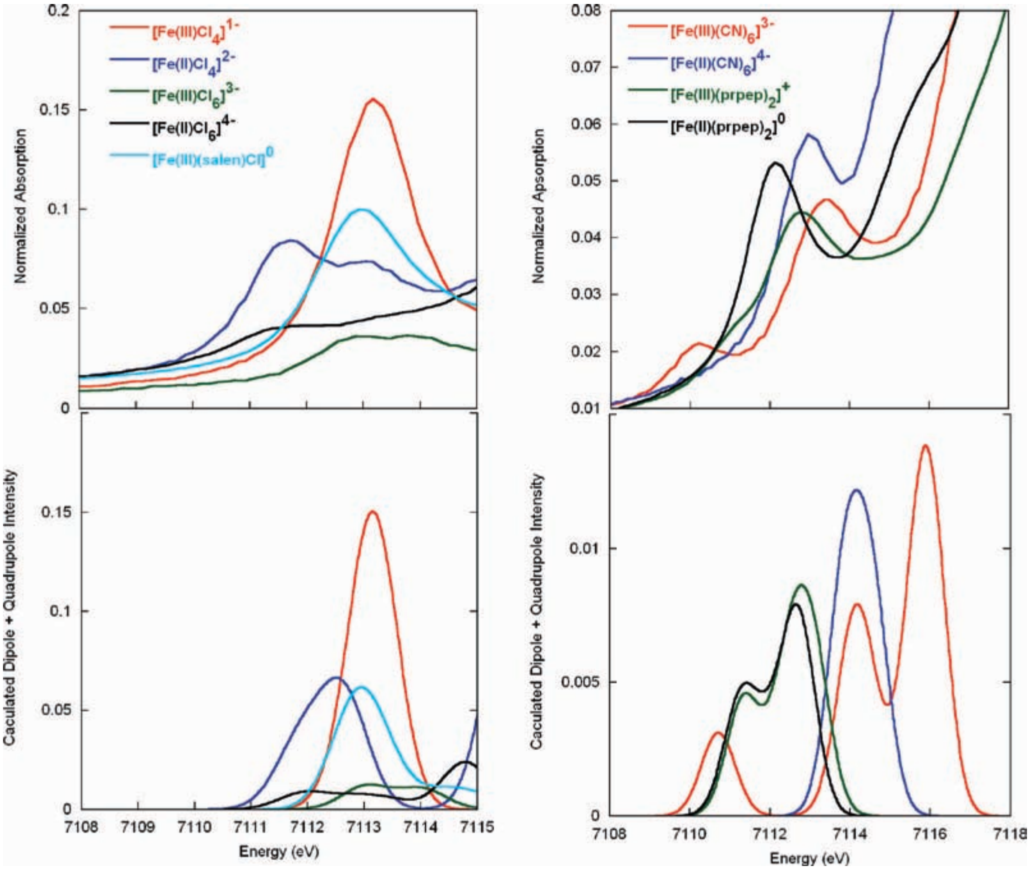

Figure 3. Experimental data for the high-spin (top, left) and low-spin (top, right) complexes, with the corresponding calculated spectra shown below. A 1 eV broadening has been applied to all calculated spectra. The experimental data for $[Fe(III)(acac)_3]^0$ were not available.

Fock (exact) exchange leads to a more correct shape of the molecular exchange-correlation potential; hence, the deviation from experiment is expected to decrease. However, this also comes at the price of a significant increase in the standard deviation of the calculated transition energies to 1.1 eV. Consideration of only complexes with neutral to dianionic total charge decreases the error in the calculated energies to 0.4 eV. This might have been expected since the virtual spectrum is strongly affected—and perhaps negatively so—through the HF exchange that leads to virtual orbitals that (incorrectly) feel a N instead of a N-1 electron potential. This is in agreement with the results obtained for Cl K-edge spectra.[19] Given the significantly higher cost of the B3LYP calculations that arises from the presence of the exact HF exchange, we conclude that B3LYP is less favorable than BP86 for the calculation of iron K-edge spectra.

Effect of Solvation (Method 3). Table 4, method 3, summarizes the results of the calculations when no solvation was included. The correlation between calculated and experimental intensity is unchanged relative to method 1. However, there is a slight (0.1 eV) increase in the error in the calculated energy. In addition, examination of the calculated spectra for $[Fe(CN)_6]^{3-/4-}$ shows that without solvation, the 1s to 3d pre-edge features have moved much closer in energy to the 1s to 4p "main" edge features, resulting in a pre-edge that is no longer resolved from the main edge. As experimentally a clear pre-edge feature is observed in these complexes, this indicates that the inclusion of solvation has led to some real improvement in the calculated spectra. This is expected since already the crude charge compensation offered by the dielectric continuum models greatly stabilizes the valence orbitals. Hence, the orbitals around the highest occupied molecular orbital (HOMO)−lowest unoccupied molecular orbital (LUMO) gap achieve positive energies and more realistic shapes as compared to the calculations that treat the naked anion in the gas phase.

Relativistic Effects (Methods 4 and 5). Methods 4 and 5, Table 4, shows the influence of scalar-relativistic effects at the level of the ZORA and DKH2 Hamiltonians, respectively. Inclusion of relativistic effects using ZORA results in a slightly larger error in the calculated intensity ($R = 0.95$). In addition, although the *absolute* energy shift required to align the calculated spectra to experimental data decreases dramatically (to 2.3 eV), the standard deviation in this values increases significantly to 2.2 eV. Consideration of complexes with a cationic to dianionic total charge improves the relative calculated energies, but the standard deviation (1.5 eV) is still much larger than that observed using method 1. This indicates that inclusion of relativistics using ZORA, although providing better *absolute* energies, results in less accurate determination of *relative* energies. We note that method 4 was also attempted using B3LYP instead of BP86. This resulted in the same error in the calculated intensities ($R = 0.95$). However, in this case, the calculated energies were overestimated relative to experiment, requiring a shift of −33.5 eV, with a standard deviation of 1.7 eV.

Inclusion of relativistics using DKH2 (method 5) results in an intensity correlation very similar to that obtained using method 1 but with a slightly larger (0.5 eV) standard deviation in the calculated energies. Clearly, the corrections in the transition energies provided by the different relativistic methods differ strongly. Both correct the calculated transition energies in the right direction. The calculated ZORA energies are within the range of the experimentally observed transition energies.

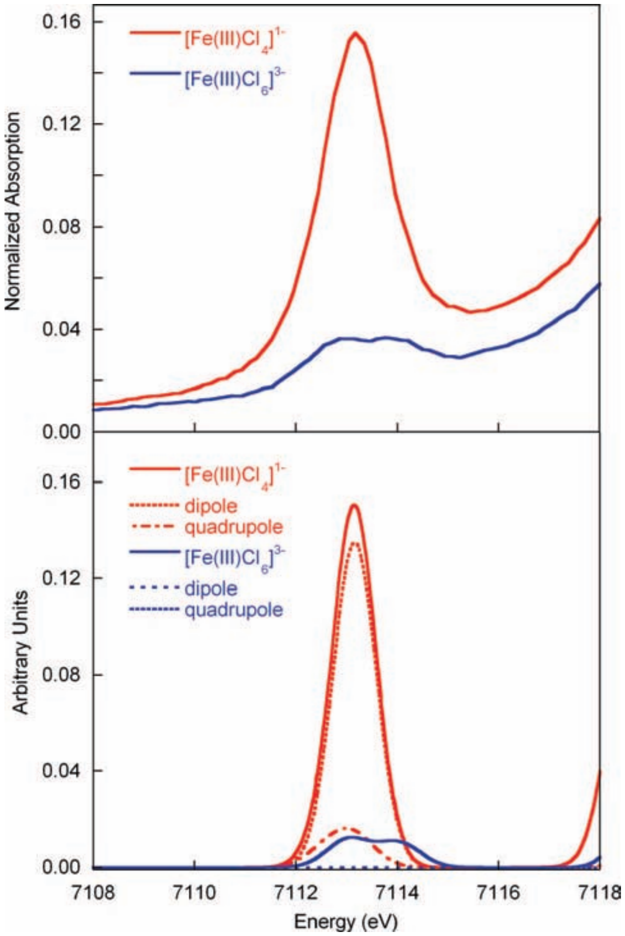

Figure 4. Comparison of experimental (top) and calculated (bottom) T_d-[Fe(III)Cl$_4$]$^{1-}$ as compared to that of O$_h$-[Fe(III)Cl$_6$]$^{3-}$, with the relative dipole and quadrupole contributions to the calculated spectra.

However, this type of agreement is fortuitous: ZORA is known to greatly overstabilize the low-lying core orbitals relative to accurate four component Dirac−Fock calculations. Hence, there is a cancelation of very large errors: the large errors in the DFT potential that shift the transition energies to too positive values and the large error in the relativistic treatment of the core that provides an opposite shift. The DKH2 procedure does not suffer from similar shortcomings. Hence, the estimate of ~30 eV shift due to relativity appears to be reasonable but of course does not remove the shortcomings of the calculated transition energies due to the reasons discussed above.

Use of Geometry Optimized Structures (Method 6). As all of the calculations were carried out as single point calculations at the crystallographic coordinates, we also investigated the impact of using geometry optimized structures. This resulted in an 0.3 eV standard deviation in the average energy shift, which was independent of the total charge on the complexes considered, and an intensity correlation, which improved to $R = 0.99$. This indicates that the correlation is equally valid for geometry optimized structures and lends confidence to using the defined method for complexes for which crystal structures are unavailable.

Dipole vs Quadrupole Contributions. Having established that method 1 results in useful agreement between calculated and experimental energies and intensities, we now examine the relative dipole vs quadrupole contributions to the pre-edge in more detail. Figure 4 shows a comparison of the experimental data for T$_d$-[Fe(III)Cl$_4$]$^{1-}$ as compared to that of O$_h$-[Fe(III)Cl$_6$]$^{3-}$ (top), with the corresponding calculated spectra and the relative dipole and quadrupole contributions (bottom). In the O$_h$ limit, the usual group theoretical selection rules dictate that only quadrupole contributions are present, and this is found in the calculations. By contrast, in T$_d$ symmetry both dipole and quadrupole 1s→3d transitions are allowed. Previous work by Westre et al. estimated that the experimental ratio of dipole to quadrupole calculation in T$_d$-[Fe(III)Cl$_4$]$^{1-}$ is ~4.2,[2] in qualitative agreement with our calculated ratio of 6.8 (Table 3, method 1). However, we note that the previous estimate assumed a constant quadrupole contribution for all ferric complexes. In the present study, we observe as much as a factor of 3 difference in the calculated quadrupole contributions over the range of ferric complexes covered here. This finding may be attributed to differences in the metal 3d character and the transition moment dipole integrals that are significantly affected by metal−ligand bonding.

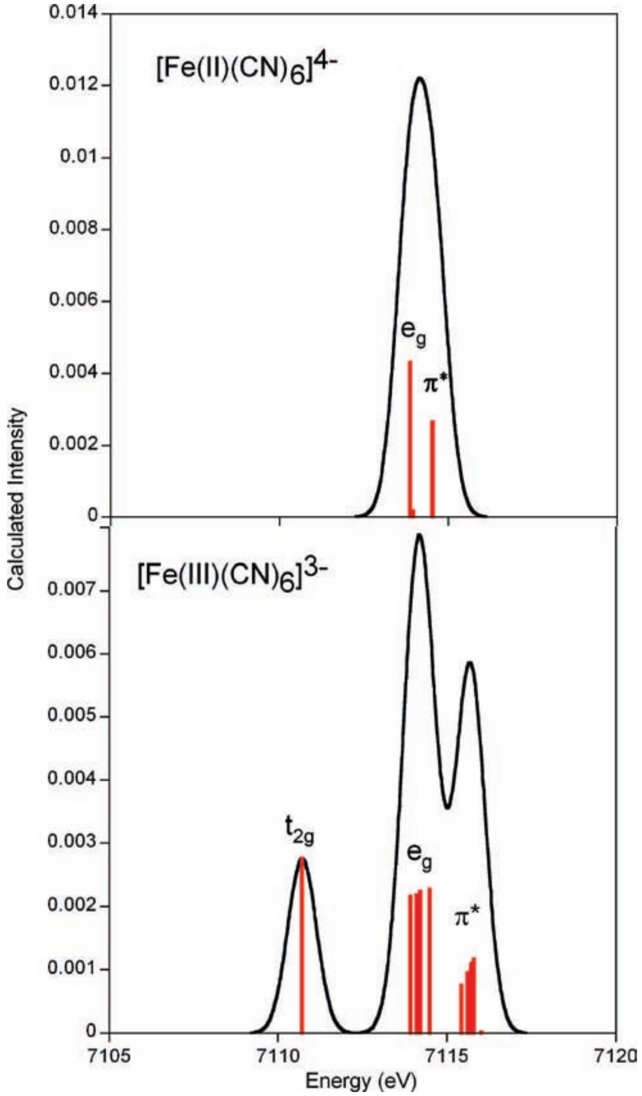

Figure 5. Comparison of the calculated spectra for [Fe(CN)$_6$]$^{4-}$ (top) and [Fe(CN)$_6$]$^{3-}$ (bottom).

Ferrous vs Ferric Hexacyanide. Despite our reservations against calculations on highly negatively charged species, we would like to report a qualitative observation on [Fe(CN)$_6$]$^{3-/4-}$ that is likely to carry over to other ferric/ferrous pairs. Figure 5 shows the calculated spectra for [Fe(CN)$_6$]$^{4-}$ and [Fe(CN)$_6$]$^{3-}$. In both cases, the spectra are dominated by quadrupole contributions, which is due to the perfect [Fe(II)] or nearly perfect [Fe(III)] O_h symmetry of the complexes. For $[Fe(CN)_6]^{4-}$, only a single peak is calculated that is comprised of transitions to the metal e_g set of d-orbitals and to the low lying π^* orbitals of the cyanide ligand. On going to $[Fe(CN)_6]^{3-}$, an additional lower energy pre-edge feature is observed, which corresponds to the promotion of the core 1s-electron into the hole in the t_{2g} set of the metal d-based molecular orbitals. In addition, the transition to the π^*-orbitals is now well-separated from the e_g transition. This is attributed to the stabilization of the metal-d manifold that is caused by the increased effective nuclear charge at the metal site in the ferric complex. The intensity of this transition therefore provides a spectral measure of backbonding, as has been previously noted in Fe L-edge studies.[46] Poorer resolution at the Fe K-edge has made observation of such features thus far prohibitive, but our calculations suggest that if XANES data could be obtained at $\sim$1 eV resolution (as is possible with current high-resolution crystal analyzer setups),[47] the Fe K-pre-edge would also provide an experimental measure of backbonding. In this respect, the present work provides a prediction to be tested in future experiments.

Discussion

In this paper, we have outlined a simple protocol for the calculation of Fe K-pre-edge features using TD-DFT.[18,19] The calculations closely follow the protocol that has previously been established for calculations of ligand K-edges.[18,19] The main modification that arises in the calculation of metal K-edges is the presence of significant quadrupole intensity. We have provided evidence above that reasonable to good agreement between calculated and experimental spectra can be obtained by using the BP86 functional with standard polarized triple-ζ basis sets such as the TZVP basis of Ahlrichs's and co-workers and the more flexible CP(PPP) basis on the iron. A small improvement in the calculated energies was seen by inclusion of solvation, which is primarily relevant for anionic species. Inclusion of scalar relativistic effects, while improving the calculated transition energies, did not lead to any better correlation with experimental spectra. Hence, these effects may be neglected in studies on 3d transition metals since the absolute calculated transition energies are in any case far from experiment because of the deficiencies of the present day DFT potentials. The relative quadrupole and dipole intensities correlate well with experimental results in the O_h to T_d limits. In addition, the ability to uniquely assign pre-edge transitions, and in some cases even to observe contributions due to backbonding, has been discussed. Higher resolution XANES data may allow for the observation of these features, which previously have only been discussed at the Fe L-edge.[46]

The present study provides a necessary calibration step. It will be important to extend our studies to the X-ray spectra of metalloprotein active sites, to unstable or short-lived reaction intermediates, and to high-valent iron complexes. The prospect of reliably calculating the XAS spectra of such systems is exciting, as has been hinted at in ref 48. Extended studies are presently underway in our laboratories.

Acknowledgment. We thank Britt Hedman, Keith Hodgson, and Ed Solomon for providing the experimental Fe K-edge data for comparison. T.P. and F.N. gratefully acknowledge financial support from the Rheinische Friedrich-Wilhelms University of Bonn and the Max-Planck Society (Max-Planck Fellowship for F.N. at the MPI for Bioinorganic Chemistry, Mülheim, Germany). SSRL operations are funded by the Department of Energy, Office of Basic Energy Sciences. The Structural Molecular Biology program is supported by the National Institutes of Health, National Center for Research Resources, Biomedical Technology Program, and the Department of Energy, Office of Biological and Environmental Research. It is our pleasure to dedicate this paper to Prof. Sason Shaik on the occasion of his 60th birthday and in recognition of his outstanding contributions to theoretical and computational chemistry.

References and Notes

(1) Roe, A. L.; Schneider, D. J.; Mayer, R. J.; Pyrz, W.; Widom, J.; Que, L., Jr. *J. Am. Chem. Soc.* **1984**, *106*, 1676.

(2) Westre, T. E.; Kennepohl, P.; DeWitt, J. G.; Hedman, B.; Hodgson, K. O.; Solomon, E. I. *J. Am. Chem. Soc.* **1997**, *119*, 6297–6314.

(3) Shulman, R. G.; Yafet, Y.; Eiseberger, P.; Blumberg, W. E. *Proc. Natl. Acad. Sci. U.S.A.* **1976**, *73*, 1384.

(4) Hahn, J. E.; Scott, R. A.; Hodgson, K. O.; Doniach, S.; Desjardins, S. R.; Solomon, E. I. *Chem. Phys. Lett.* **1982**, 595–598.

(5) Dräger, G.; Frahm, R.; Materlik, G.; Brümmer, O. *Phys. Stat. Solidi B* **1988**, *146*, 287.

(6) Penner-Hahn, J. E. *Coord. Chem. Rev.* **2005**, *249*, 161.

(7) Arrio, M.-A.; Rossano, S.; Brouder, C.; Galoisy, L.; Calas, G. *Europhys. Lett.* **2000**, *51* (4), 454.

(8) Wasinger, E. C.; Davis, M. I.; Pau, M. Y. M.; Orville, A. M.; Zaleski, J. M.; Hedman, B.; Lipscomb, J. D.; Hodgson, K. O.; Solomon, E. I. *Inorg. Chem.* **2003**, *42*, 265.

(9) Kemsley, J. N.; Zaleski, K. L.; Chow, M. S.; Decker, A.; Shishova, E. Y.; Wasinger, E. C.; Hedman, B.; Hodgson, K. O.; Solomon, E. I. *J. Am. Chem. Soc.* **2003**, *125*, 10810.

(10) Solomon, E. I.; Brunold, T. C.; Davis, M. I.; Kemsley, J. N.; Lee, S.-K.; Lehnert, N.; Neese, F.; Skulan, A. J.; Yang, Y.-S.; Zhou, J. *Chem. Rev.* **2000**, *100*, 235.

(11) Aliaga-Alcalde, N.; DeBeer George, S.; Mienert, B.; Bill, E.; Wieghardt, K.; Neese, F. *Angew. Chem., Int. Ed.* **2005**, *44*, 2908.

(12) Berry, J. F.; Bill, E.; Bothe, E.; DeBeer George, S.; Mienert, B.; Neese, F.; Wieghardt, K. *Science* **2006**, *312*, 1937.

(13) Chanda, A.; Shan, X.; Chakrabarti, M.; Ellis, W. C.; Popescu, D. L.; Tiago de Oliveira, F.; Wang, D.; Que, L., Jr.; Collins, T. J.; Münck, E.; Bominaar, E. L.; Chem, I. *Inorg. Chem.* 2008.

(14) Lim, M. H.; Rohde, J.-U.; Stubna, A.; Bukowski, M. R.; Costas, M.; Ho, R. Y. N.; Münck, E.; Nam, W. L.; Que, J. *Proc. Natl. Acad. Sci. U.S.A.* **2003**, *100*, 3665.

(15) Oliveira, F. T. d.; Chanda, A.; Banerjee, D.; Shan, X. P.; Mondal, S. L. Q., Jr.; Bominaar, E. L.; Münck, E.; Collins, T. J. *Science* **2007**, *315*, 835.

(16) Rohde, J.-U.; Betley, T. A.; Jackson, T. A.; Saouma, C. T.; Peters, J. C.; Que, L., Jr. *Inorg. Chem.* **2007**, *46*, 5720.

(17) DeBeer George, S.; Brant, P.; Solomon, E. I. *J. Am. Chem. Soc.* **2005**, *127*, 667.

(18) DeBeer George, S.; Petrenko, T.; Neese, F. *Inorg. Chim. Acta* **2008**, *361*, 965.

(19) Ray, K.; DeBeer George, S.; Solomon, E. I.; Wieghardt, K.; Neese, F. *Chem. Eur. J.* **2007**, *13*, 2783.

(20) Dreuw, A.; Head-Gordon, M. *Chem. Rev.* **2005**, *105* (11), 4009–4037.

(21) Neese, F. *Coord. Chem. Rev.* **2008**, ASAP (DOI: 10.1016/j.ccr.2008.05.014).

(22) Hirata, S.; Head-Gordon, M. *Chem. Phys. Lett.* **1999**, *314* (3−4), 291–299.

(23) Grimme, S.; Neese, F. *J. Chem. Phys.* **2007**, *127*, 154116.

(24) Neese, F.; Olbrich, G. *Chem. Phys. Lett.* **2002**, *362* (1−2), 170–178.

(25) Neese, F. *ORCA—An Ab Initio, DFT, and Semiempirical Electronic Structure Package*, Version 2.6.35; University of Bonn: Germany, 2008.

(26) Kistenmacher, T. J.; Stucky, G. D. *Inorg. Chem.* **1967**, *7*, 2150.

(27) Lauher, J. W.; Ibers, J. A. *Inorg. Chem.* **1975**, *14*, 348.

(28) Beattie, J. K.; Moore, C. J. *Inorg. Chem.* **1982**, *21*, 1292.

(29) Iball, J.; Morgan, C. H. *Acta Crystallogr.* **1967**, *23*, 239.

(30) Gerloch, M.; Mabbs, F. E. *J. Chem. Soc. A* **1967**, 1598.

(31) Overgaard, J.; Svendsen, H.; Chevalier, M. A.; Iversen, B. B. *Acta Crystallogr.* **2005**, *E61*, m268–m270.

(32) Kuchár, J.; Cernák, J.; Massa, W. *Acta Crystallogr.* **2004**, *C60*, m418–m420.

(33) Brown, S. J.; Olmstead, M. M.; Mascharak, P. K. *Inorg. Chem.* **1990**, *29*, 3229.

(34) Becke, A. D. *Phys. Rev. A* **1988**, *38*, 3098.

(35) Perdew, J. P. *Phys. Rev. B* **1986**, *33*, 8822.

(36) Neese, F. *Inorg. Chim. Acta* **2002**, *337C*, 181.

(37) Schäfer, A.; Huber, C.; Ahlrichs, R. *J. Chem. Phys.* **1994**, *100*, 5829.

(38) Klamt, A.; Schüürmann, G. *J. Chem. Soc. Perkin Trans.* **1993**, *2*, 799–805.

(39) Van Wüllen, C. *J. Chem. Phys.* **1998**, *109*, 382.

(40) Hess, B. A. *Phys. Rev. A* **1986**, *33*, 3742.

(41) Jansen, G.; Hess, B. A. *Phys. Rev. A* **1989**, *39*, 6016.

(42) Note that the fit line in Figure 1 has a non-zero intercept (of ∼2 units of experimental intensity). This may indicate that the quadrupole contribution is underestimated by the calculation and/or that there are additional contributions to the experimental data besides the quadrupole and dipole contributions. Previous work by Hahn et al. (*Chem. Phys. Lett.* **1982**, *88*, 595) on the angular dependent absorption spectra of $[CuCl_4]^{2-}$ have noted a small but constant offset to the data that was attributed to possible vibronic coupling. Such contributions are not accounted for in the present model, although this could be addressed experimentally through temperature-dependent studies. The fit line in Figure 1 has a non-zero intercept (of ∼2 units of experimental intensity).

(43) van Leeuwen, R.; Gritsenko, O. V.; Baerends, E. J. Analysis and modelling of atomic and molecular Kohn-Sham potentials. In *Density Functional Theory I*; Springer: New York, 1996; Vol. 180, pp 107−167.

(44) Hess, B. A.; Marian, C. M. Relativistic methods review. In *Computational Molecular Spectroscopy*; Jensen, P., Bunker, P. R., Eds.; John Wiley & Sons: New York, 2000; p 169ff.

(45) Janetzko, F.; Köster, A. M.; Salahub, D. R. *J. Chem. Phys.* **2008**, *128*, 024102.

(46) Hocking, R. K.; Wasinger, E. C.; de Groot, F. M. F.; Hodgson, K. O.; Hedman, B.; Solomon, E. I. *J. Am. Chem. Soc.* **2006**, *128*, 10442.

(47) Glatzel, P.; Bergmann, U. *Coord. Chem. Rev.* **2005**, *249*, 65.

(48) Berry, J. F.; DeBeer George, S.; Neese, F. *Phys. Chem. Chem. Phys.* **2008**, *10*, 4361–4374.

JP803174M